RSC Advances

PAPER

View Article Online
View Journal | View Issue

Cite this: *RSC Adv.*, 2021, **11**, 4138

First cycloruthenation of 2-alkenylpyridines: synthesis, characterization and properties†

Yuhao Wu,‡[a] Xianlong Su,‡[a] Chaoyi Xie,[a] Rongrong Hu,[b] Xianghong Li,*[a] Qiang Zhao,[b] Guoli Zheng[a] and Junkun Yan[a]

Received 19th November 2020
Accepted 5th January 2021

DOI: 10.1039/d0ra09833g

rsc.li/rsc-advances

Several cyclometalated ruthenium complexes **1–5** with 2-alkenylpyridines as *C*,*N*-chelating ligands were synthesized and then characterized by NMR, MS, IR and UV-Vis spectra. According to the single crystal of complex **2**, it is evident that carbon from vinyl group is successfully bonded to Ru(II) center. Moreover, the Ru–N bond trans to the Ru–C bond is elongated (2.127(5) Å), which is consistent with the strong trans effect of the carbon atom compared to that of the nitrogen atom. With different electron-donating groups linked to vinyl, these complexes exhibited regular changes in MLCT absorption bands, which were identified by UV-Vis and CV spectra in combination with DFT and TD-DFT. Interestingly, protonated intermediate species of these complexes in acidic solutions were tracked by the absorption changes and MS spectra, which displayed a possible protonation process of these complexes with the cleavage of Ru–C σ bonds.

Introduction

Cyclometalated complexes have attracted considerable interest for a wide variety of applications,[1] since the first cyclometalated platinum complex was reported in 1965.[2] There are now many examples of reactions involving metalation of ligands by transition metals such as Ir(III), Rh(III), Pt(IV), Ru(II), and Os(II). It is noted that the metalated ligand should contain at least one common donor atom (N, P, O, S) and one carbon donor atom.[3] The carbon donor atoms usually involve alkyl,[4] aryl,[5] or benzyl.[4,6] In comparison with aryl carbons, the metalation of alkenyl carbons is much less common. Up to now, some transition metals such as rhodium,[7] platinum[8] and iridium[9] have been reported by metalations at alkenyl carbons involving 2-vinylpyridines.

Cyclometalated ruthenium complexes have been investigated for their significantly improved absorptions in the visible region especially when compared with the classic $Ru(bpy)_3^{2+}$.[10,11] To date, many cycloruthenated complexes have been synthesized and used as energy acceptors,[12] electron transfer sensitizers in dyads,[13] redox mediators in oxidase chemistry,[14] sensitizers for dye sensitized solar cells,[15] chemosensors,[16] and PDT sensitizers[17] by personalized modifications of cyclometalated ligands such as expanding π-systems,[13,15] and grafting photosensitive groups.[16b,17] However, most of ligand frameworks used in these complexes have been based on 2-arylpyridine derivatives[11–17] and *N*-heterocyclic carbenes[18] with rare examples with 2-phenylimidazole,[19] and *N*,*N*-dimethylbenzylamine.[14b,20] To the best of our knowledge, few cycloruthenations of 2-vinylpyridine and derivatives have been reported.

Therefore, our interest in the design of new organic ligands for cyclometalated ruthenium complexes has led us to synthesize a series of 2-alkenylpyridines. Herein, we investigated in details a series of ruthenium(II) metalations at alkenyl carbons involving 2-alkenylpyridine and related ligands. The synthetic route is shown in Scheme 1. After being characterized by NMR, MS, FT-IR and elemental analysis, photophysical properties of these complexes were investigated by UV-Vis and FL spectra in combination with CV spectra and theoretical calculations. To the best of our knowledge, deprotonations of ligands are necessary for the formation of cyclometalated ruthenium complexes. However, there have been rare examples on the protonation of cycloruthenated complexes despite that. Therefore, these complexes incubated in acidic solutions were investigated in details. Then, possible acid–base equilibria for these complexes were depicted.

Experimental sections

Materials

Ethyltriphenylphosphonium bromide, benzyltriphenylphosphonium bromide, triphenyl-(4-fluorobenzyl)phosphonium bromide, triphenyl-(4-*N*,*N*-dimethylbenzyl)phosphonium bromide, and triphenyl-(thiophen-2-ylmethyl)phosphonium bromide were prepared

[a]*Key Laboratory of Catalysis and Energy Materials Chemistry of Ministry of Education, Hubei Key Laboratory of Catalysis and Materials Science, South-Central University for Nationalities, Wuhan 430074, China. E-mail: lixhchem@mail.scuec.edu.cn*

[b]*Key Laboratory for Organic Electronics & Information Displays (KLOEID), Institute of Advanced Materials (IAM), Nanjing University of Posts & Telecommunications (NUPT), Nanjing 210023, China*

† Electronic supplementary information (ESI) available: Additional spectral data associated with this article can be found. CCDC 2032477 containing the supplementary crystallographic data for complex **2**. For ESI and crystallographic data in CIF or other electronic format see DOI: 10.1039/d0ra09833g

‡ These authors contributed equally.

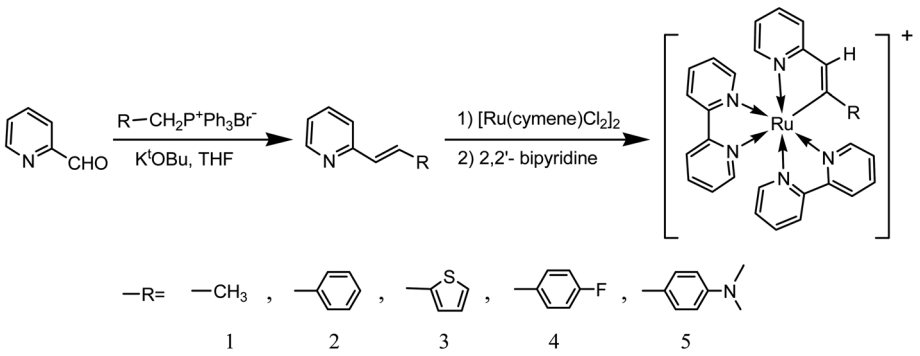

Scheme 1 The reactions of 2-alkenylpyridine and related ligands with ruthenium(II).

by the methods described in literatures[21] and used directly in the synthesis of 2-vinylpyridine derivatives. All solvents and reagents were commercially available and used without further purification unless specified.

Physical measurements

NMR spectra were recorded on a Bruker Avance-400 spectrometer. Mass spectra were obtained on a Bruker autoflex speed MALDI-TOF spectrometer by using CHCA (α-cyano-4-hydroxycinnamic acid) as matrix and elemental analyses were determined by a VarioEL III O-Element Analyzer system. Absorption spectra were recorded using a Shimadzu UV-2550 spectrophotometer. Fluorescence spectra were recorded on a Varian Cary Eclipse spectrophotometer in a 4.5 mL (1 cm in diameter) cuvette with 2 mL solution at 77 K. All pH measurements were made with a Model pHS-3B pH meter (Shanghai, China). Cyclic voltammogram spectra of **1–5** were collected in MeCN with $[n\text{-}Bu_4N]PF_6$ as the supporting electrolyte at 100 mV s^{-1}, using the standard three-electrode setup with a platinum disk as working electrode, platinum wire as counter electrode, and $AgNO_3$/Ag as reference electrode. Herein, potentials reported relative *vs.* ferrocenium/ferrocene (Fc^+/Fc) used as an internal standard. The single-crystal X-ray data were collected on a Bruker P4 diffractometer with Mo Kα radiation ($\lambda = 0.71073$ Å) using the ω-scan mode. The crystal of **2** was kept at a steady $T = 293(2)$ K during data collection. The structure of **2** was solved with the Olex2.solve[22a] solution program by using Olex2 1.3-dev[22b] as the graphical interface. The model was refined with ShelXL 2018/3 (ref. 22*c*) using full matrix least squares minimization on F^2.

Preparation of solutions

Deionized water was used throughout all experiments. Stock solutions of 2-alkenylpyridine ligands (1.0 mM) and complexes **1–5** were prepared in acetonitrile and ethanol, respectively. Then, solutions of 2-alkenylpyridine ligands were diluted to 20 μM with acetonitrile, while complexes were diluted to 20 μM with ethanol. For complexes **1–5**, their buffered solutions were prepared in ethanol and Briton–Robinson buffer at volume ratio of 1 : 2 and then incubated for 4 h.

Theoretical calculations

All the density functional theory (DFT) and time-dependent density functional theory (TD-DFT) calculations were performed with the Gaussian 09 package.[23] The structures in the ground state (S_0) were fully optimized by the Becke's three-parameter exchange functional along with the Lee–Yang–Parr correlation functional (B3LYP) and plus polarization function 6-31G* basis set. Calculations of electronic absorption spectra were computed with the time-dependent density functional theory (TD-DFT) method at the B3LYP/6-31G* level based on the optimized ground-state structures. For all the calculations, the associated basis set was applied to describe Ru with the "double-ζ" quality LANL2DZ basis set, whereas, for all other atoms, the 6-31G(d) basis set was employed. The contours of the HOMOs and LUMOs orbitals were plotted.

Synthesis of ligands

(*E*)-2-(Prop-1-en-1-yl)pyridine. In a three-necked flask, 2-pyridylaldehyde (45.6 mg, 0.43 mmol) and anhydrous ^{t}BuOK (98.7 mg, 0.88 mmol) were dried in vacuum for 30 min and followed by adding 20 mL of dry THF. Then, ethyltriphenylphosphonium bromide (160.2 mg, 0.43 mmol) dissolved in 5 mL of dry THF was added dropwise to the above solution with stirring under N_2 atmosphere. The mixture was stirred at ambient temperature for another 3 h and then poured into ice-water (40 mL). The mixture was extracted with dichloromethane and concentrated in vacuum. After purified by silica gel column chromatography with CH_2Cl_2/petroleum ether (v/v = 2 : 1) as eluent, orange oil was obtained with yield of 61% (0.031 g). The ^{1}HNMR was in good agreements with the ref. 9*a*.

(*E*)-2-Styrylpyridine. The procedure was the same as that of (*E*)-2-(prop-1-en-1-yl)pyridine. Yield: 0.052 g (67%). ^{1}H NMR ($CDCl_3$, 400 MHz), δ (ppm): 8.61 (d, $J = 4.4$ Hz, 1H), 7.48 (td, $J = 8.0$ Hz, $J = 2.0$ Hz 1H), 7.27–7.25 (m, 5H), 7.19 (d, $J = 8.0$ Hz, 1H), 7.12–7.09 (m, 1H), 6.87 (d, $J = 12.4$ Hz, 1H), 6.73 (d, $J = 12.4$ Hz, 1H).

(*E*)-2-(2-(Thiophen-2-yl)vinyl)pyridine. Yield: 0.046 g (58%). ^{1}H NMR ($CDCl_3$, 400 MHz), δ (ppm): 8.73 (d, $J = 4.0$ Hz, 1H), 7.68 (td, $J = 1.6$ Hz, $J = 7.8$ Hz, 1H), 7.35 (d, $J = 7.8$ Hz, 1H), 7.29 (d, $J = 4.0$ Hz, 1H), 7.25 (d, $J = 3.6$ Hz, 1H), 7.19 (dd, $J = 7.8$ Hz, $J = 4.8$ Hz, 1H), 7.00 (dd, $J = 7.2$ Hz, $J = 3.6$ Hz, 1H), 6.92 (d, $J = 12.4$ Hz, 1H), 6.51 (d, $J = 12.4$ Hz, 1H).

(*E*)-2-(4-Fluorostyryl)pyridine. Yield: 0.053 g (62%). ^{1}H NMR (CD_3OD, 400 MHz), δ (ppm): 8.51 (d, $J = 5.2$ Hz, 1H), 7.66–7.63 (m, 1H), 7.28–7.21 (m, 4H), 7.01–6.96 (m, 2H), 6.89 (d, $J = 12.1$ Hz, 1H), 6.70 (d, $J = 12.1$ Hz, 1H).

(*E*)-*N*,*N*-Dimethyl-4-(2-(pyridin-2-yl)vinyl)aniline. Yield: 0.044 g (46%). ^{1}H NMR ($CDCl_3$, 400 MHz), δ (ppm): 8.59 (s, 1H),

7.64–7.49 (m, 4H), 7.37 (d, J = 7.6 Hz, 1H), 7.09 (s, 1H), 7.03 (d, J = 16.0 Hz, 1H), 6.75 (d, J = 8.4 Hz, 2H), 3.02 (s, 6H).

Preparation of complexes

A suspension of $[Ru(cymene)Cl_2]_2$ (0.16 g, 0.26 mmol), triethylamine (0.05 mL), 2-vinylpyridine derivative (0.50 mmol) and KPF_6 (0.182 g, 0.99 mmol) in 10 mL of acetonitrile was stirred at 50 °C for 24 h under argon. Then, the solvent was removed under vacuum. The orange red solid was obtained and added into the methanol solution (10 mL) containing 2,2′-bipyridine (0.169 g, 1.08 mmol). After the solution was refluxed for 2 h under argon, the solvent was removed by evaporation. The crude compound was purified directly by column chromatography on silica gel using CH_3CN/CH_2Cl_2 as eluent to afford the product as black solid.

1. Yield: 0.079 g (45%). ^{1}HNMR (CD_3CN, 400 MHz), δ (ppm): 8.48 (dd, J = 5.6 Hz, J = 0.8 Hz, 1H), 8.45 (d, J = 8.0 Hz, 1H), 8.39 (d, J = 8.0 Hz, 1H), 8.35 (d, J = 8.0 Hz, 1H), 8.30 (d, J = 8.0 Hz, 1H), 7.99 (td, J = 8.0 Hz, J = 1.6 Hz, 1H), 7.91–7.85 (m, 2H), 7.82–7.77 (m, 1H), 7.74 (dd, J = 5.6 Hz, 2H), 7.68 (d, J = 5.6 Hz, 1H), 7.47 (td, J = 8.0 Hz, J = 1.6 Hz, 1H), 7.42–7.37 (m, 2H), 7.34 (m, 1H), 7.28–7.26 (m, 2H), 7.18–7.14 (m, 1H), 7.04 (d, J = 1.2 Hz, 1H), 6.60 (td, J = 7.2 Hz, J = 1.2 Hz, 1H), 1.84 (d, J = 1.2 Hz, 3H). ^{13}CNMR (CD_3CN, 100 MHz), δ (ppm): 215.54, 169.35, 157.54, 156.99, 156.79, 154.96, 154.71, 150.63, 149.99, 149.35, 148.68, 136.34, 134.94, 134.78, 133.67, 133.54, 126.87, 126.77, 126.37, 126.18, 125.86, 123.28, 122.95, 122.74, 122.60, 118.56, 117.30, 27.66. MS (Maldi-TOF, CHCA): m/z calculated for 532.11 (M-PF_6^-), found: 532.06. $C_{28}H_{24}F_6N_5PRu$ calc. C, 49.71; H, 3.58; N, 10.35; found C, 50.06; H, 3.35; N, 10.43.

2. Yield: 0.058 g (30%). ^{1}H NMR (CD_3CN, 400 MHz), δ (ppm): 8.89 (d, J = 8.0 Hz, 1H), 8.47 (dd, J = 8.0 Hz, 2H), 8.19 (d, J = 8.0 Hz, 1H), 7.99–7.86 (m, 4H), 7.76 (d, J = 5.4 Hz, 1H), 7.71 (d, J = 5.4 Hz, 1H), 7.57–7.44 (m, 5H),7.39–7.35 (m, 3H), 7.13 (s, 1H), 6.98 (td, J = 8.0 Hz, J = 1.6 Hz, 1H), 6.85–6.83 (m, 3H), 6.69 (td, J = 8.0 Hz, J = 1.6 Hz, 1H), 6.43 (dd, J = 1.6 Hz, 2H). ^{13}CNMR (CD_3CN, 100 MHz), δ (ppm): 200.14, 169.49, 157.50, 156.94, 156.55, 155.53, 155.05, 151.59, 150.85, 150.07, 149.62, 148.91, 136.54, 135.24, 135.13, 133.95, 133.55, 129.74, 128.42, 128.17, 127.15, 126.91, 126.41, 126.08, 126.01, 125.67, 124.33, 123.46, 123.09, 122.35, 122.31, 120.07, 119.65, 118.34. MS (Maldi-TOF, CHCA): m/z calculated for 594.12 (M-PF_6^-), found: 594.09. $C_{33}H_{26}F_6N_5PRu$ calc. C, 53.66; H, 3.55; N, 9.48; found C, 52.96; H, 3.35; N, 10.02.

3. Yield: 0.052 g (27%). ^{1}H NMR (CD_3CN, 400 MHz): 8.69 (d, J = 5.6 Hz, 1H), 8.44 (dd, J = 8.0 Hz, 2H), 8.28 (dd, J = 8.0 Hz, 2H), 7.99 (t, J = 8.0 Hz, 1H), 7.89 (dd, J = 8.0 Hz, 2H), 7.77 (t, J = 7.2 Hz, 1H), 7.67–7.65 (m, 3H), 7.54–7.28 (m, 7H), 7.13 (t, J = 6.8 Hz, 1H), 7.02 (d, J = 5.2 Hz, 1H), 6.65 (d, J = 5.6 Hz, 2H), 6.09 (d, J = 3.6 Hz, 1H); ^{13}CNMR (CD_3CN, 100 MHz), δ (ppm): 207.76, 168.92, 157.52, 156.96, 156.84, 155.56, 155.16, 154.20, 150.88, 150.27, 149.61, 148.87, 136.80, 135.32, 135.21, 134.18, 134.05, 129.38, 127.28, 127.12, 126.58, 126.15, 126.02, 123.97, 123.52, 123.20, 122.82, 122.63, 122.52, 120.30, 118.29. MS (Maldi-TOF, CHCA): m/z calculated for 600.03 (M-PF_6^-), found: 600.10. $C_{31}H_{24}F_6N_5PRuS$ calc. C, 50.00; H, 3.25; N, 9.40. Found: C, 49.75; H, 3.64; N, 9.07.

4. Yield: 0.049 g (25%). ^{1}HNMR (CD_3CN, 400 MHz), δ (ppm): 8.84 (d, J = 5.2 Hz, 1H), 8.47–8.42 (dd, J = 8.0 Hz, 2H), 8.19 (d, J = 8.4 Hz, 1H), 8.02–7.87 (m, 4H), 7.74 (dd, J = 5.2 Hz, 2H), 7.62–7.51 (m, 3H), 7.47–7.35 (m, 5H), 7.14 (s, 1H), 7.01 (t, J = 7.2 Hz, 1H), 6.71–6.68 (m, 1H), 6.60 (t, J = 8.8 Hz, 2H), 6.43 (m, 2H); ^{13}CNMR (d_6-DMSO, 125 MHz), δ (ppm): 198.87, 169.18, 159.22, 157.39, 156.88, 156.56, 155.55, 155.03, 150.69, 149.92, 149.57, 148.91, 148.02, 137.31, 135.85, 135.72, 134.77, 134.42, 129.06, 127.83, 127.33, 126.95, 126.64, 125.31, 125.25, 124.32, 123.91, 123.30, 123.22, 120.66, 119.18, 114.31, 114.15. MS (Maldi-TOF, CHCA): m/z calculated for 612.09 (M-PF_6^-), found: 612.16. $C_{33}H_{25}F_7N_5PRu$ calc. C, 52.38; H, 3.33; N, 9.26; found: C, 52.05; H, 3.84; N, 9.73.

5. Yield: 0.051 g (25%). ^{1}H NMR (CD_3CN, 400 MHz), δ (ppm): 8.79 (d, J = 5.6 Hz, 1H), 8.46 (dd, J = 8.0 Hz, 2H), 8.20 (d, J = 8.0 Hz, 1H), 8.07 (d, J = 8.0 Hz, 1H), 7.97 (td, J = 7.2 Hz, J = 1.6 Hz, 1H), 7.89–7.83 (m, 2H), 7.73 (d, J = 5.6 Hz, 1H), 7.67–7.62 (m, 2H), 7.59 (d, J = 5.6 Hz, 1H), 7.49 (td, J = 8.0 Hz, J = 1.6 Hz, 1H), 7.40–7.29 (m, 5H), 7.11 (s, 1H), 7.03 (t, J = 6.4 Hz, 1H), 6.62 (t, J = 6.4 Hz, 1H), 6.46 (d, J = 8.0 Hz, 2H), 6.29 (d, J = 8.0 Hz, 2H), 2.76 (s, 6H); ^{13}CNMR (d_6-DMSO, 125 MHz), δ (ppm): 221.47, 167.33, 155.37, 154.75, 154.53, 153.51, 152.88, 148.51, 147.78, 147.20, 146.76, 146.48, 137.75, 135.11, 133.54, 133.30, 132.16, 132.10, 125.76, 125.41, 125.04, 124.58, 124.40, 123.68, 122.11, 121.71, 121.25, 121.11, 117.98, 116.03, 29.49, 28.16. MS (Maldi-TOF, CHCA): m/z calculated for 637.17 (M-PF_6^-), found: 637.12. $C_{35}H_{31}F_6N_6PRu$ calc. C, 53.78; H, 4.00; N, 10.75; found: C, 53.55; H, 4.44; N, 10.93.

Results and discussion

Synthesis and characterization

The synthetic route of complexes **1–5** is presented in Scheme 1. Herein, 2-vinylpyridine derivatives involving different electron-withdrawing groups were firstly prepared by Wittig reactions between their corresponding phosphonium bromides and 2-pyridylaldehyde in the presence of *t*-BuOK with the moderate yields (46–67%), which were characterized by ^{1}HNMR spectra (Fig. S1–S4†). Then, trimethylamine[24] was used as a deprotonating agent to get their corresponding cyclometalated ruthenium complexes without purifying intermediates. And the yields were still satisfied in the range from 25 to 45%. All these complexes were characterized by NMR (Fig S5–S14†), MS (Fig. S5–S9† inset), IR (Fig. S15†) and elemental analysis spectra. It should be noted that the peaks attributed to Ru–C in ^{13}CNMR spectra of these complexes were clearly observed in the range from 198 to 222 ppm, which are in accordance with those of $[RuL(bpy)_2]PF_6$ indicating successful cyloruthenations of these 2-vinylpyridine derivatives.[11–17] Moreover, all the MS spectra of these complexes showed the parent peaks with the loss of one counter ion, which are in good agreements with the structures.

A single-crystal of **2** suitable for X-ray analysis was obtained by slow diffusion of petroleum ether into a solution of **2** in methanol. Then, complex **2** was further identified by X-ray crystallographic analysis. The structure of **2** is shown in Fig. 1. Further details of the crystal data, data collection, structure solution, and refinement parameters were summarized in Table S1.† Selected bond distances and angles were collected in Table 1. Herein, **2** adopts a triclinic, distorted octahedral coordination around the Ru(II) center with two

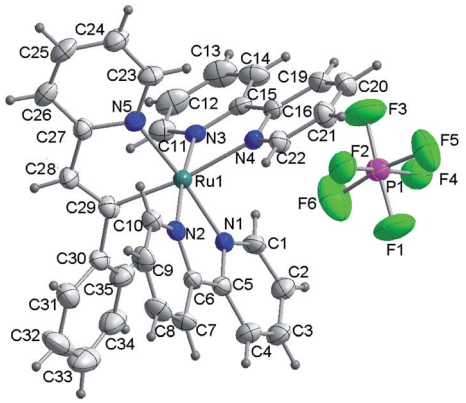

Fig. 1 ORTEP representation of the X-ray structure of complex **2**. Herein, CH_3OH is omitted for clarity.

chelating bipyridines and one (*N*,*C*)-bidentate ligand. The C(29)–Ru(1)–N(4) deviates slightly from linearity with the corresponding angle of 172.0(3)°. Along this line, the Ru(1)–C(29) bond was measured to be 2.037(7) Å, in the range of Ru–C distances observed for similar complexes.[25] The Ru(1)–N(4) bond trans to the Ru(1)–C(29) bond is too elongated (2.127(5) Å) with respect to the Ru–N distances observed for bipyridine N(1) and N(2) atoms (2.047(5) and 2.056(6) Å, respectively). The result is consistent with the strong trans effect of the carbon atom compared with that of the nitrogen atom. However, it should be noted that the Ru(1)–N(5) bond is also somewhat elongated (2.067(5) Å).

Photophysical properties

The spectroscopic properties of complexes **1–5** were investigated in details. As shown in Fig. 2 and Table 2, all these complexes display several absorption bands in UV-Vis spectral regions. According to the absorption spectra of these 2-alkenylpyridines in Fig. S16,† the bands between 300 and 450 nm can be assigned as LC transitions of 2-vinylpyridine derivatives mixed with LMCT transitions. The bands occurring between 450 and 800 nm are assigned as MLCT transitions. The first intense absorption band was observed at about 490 nm for these complexes, which is assigned as Ru(II) → cyclometalated ligands CT. The second intense absorption band was observed around 530 nm, which is assigned as Ru(II) → bpy CT transitions and noticeably red-shifted relative to $Ru(bpy)_3^{2+}$ derivatives. Compared with absorptions of 2-alkenylpyridines, this red-shift can be attributed to the formation of Ru–C bond,[11,25] which clearly indicated that ruthenations at alkenyl carbons involving 2-vinylpyridine derivatives were successful. In comparison with complex **1**, the MLCT absorptions attributed to Ru(II) → bpy CT transitions are blue-shifted when methyl linked to vinyl was substituted by aryl such as 2-thienyl and phenyl derivatives. However, it should be noted that molar extinction coefficients of these complexes increased when aryl groups were linked to vinyl, as shown in Fig. 2 and Table 2. In addition, when electron donating or withdrawing groups were linked to phenyl in vinylphenyl parts, the absorption properties were also altered. As shown in Fig. 2 inset, Ru(II) → bpy CT transitions of complex **2** are centered at 527 nm while those of complex **4** with electron withdrawing group are centered at 524 nm. However, for complex **5** with *N*,*N*-dimethyl, the maximum absorption peak is centered at 538 nm. The results may be due to the different electron distributions on complexes induced by these groups. Nevertheless, there were no strong emissive spectra observed upon excited at ambient temperature. Then, the emission spectra at 77 K were investigated. As shown in Fig. S17,† the maximum emission peaks of complexes **1–5** are centered at 774, 710, 707, 708 and 726 nm, respectively. The results are in agreements with the regular changes of absorptions.

Electrochemical behaviors

The electrochemical behaviors of complexes **1–5** have been studied *via* cyclic voltammetry (CV) (Fig. S18†) and the summarized data are listed in Table 3. In the positive charge region, oxidation peaks attributed to $Ru^{2+/3+}$ and anionic *C*,*N*-

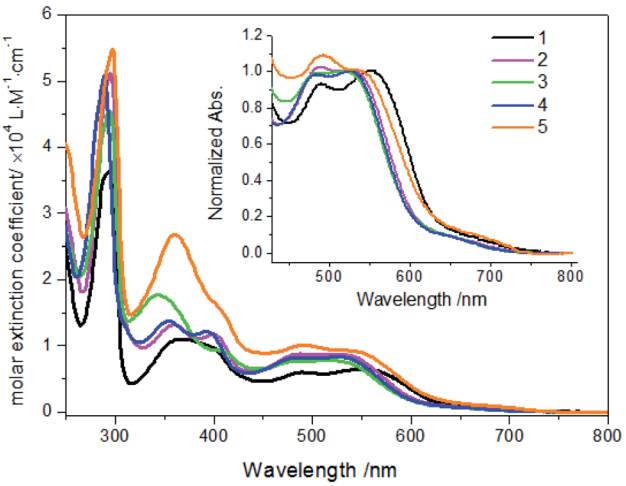

Fig. 2 Absorption spectra of complexes **1–5** (20 μM) in ethanol solution. Inset: normalized absorption spectra of complexes.

Table 1 Selected bond lengths [Å] and angles [°] for **2**

Ru(1)–N(1)	2.047(5)	Ru(1)–N(2)	2.056(6)	Ru(1)–N(3)	2.056(6)
Ru(1)–N(4)	2.127(5)	Ru(1)–N(5)	2.067(5)	Ru(1)–C(29)	2.037(7)
C(28)–C(29)	1.345(10)	C(29)–C(30)	1.490(10)	C(29)–Ru(1)–N(4)	172.0(3)
C(5)–N(1)–C(1)	117.6(6)	C(1)–N(1)–Ru(1)	126.4(5)	C(5)–N(1)–Ru(1)	116.0(5)
C(6)–N(2)–Ru(1)	115.4(5)	C(10)–N(2)–Ru(1)	126.6(5)	C(11)–N(3)–Ru(1)	125.7(5)
C(15)–N(3)–Ru(1)	116.5(5)	C(16)–N(4)–Ru(1)	115.2(5)	C(27)–N(5)–Ru(1)	115.5(5)
C(28)–C(29)–Ru(1)	114.4(6)	C(30)–C(29)–Ru(1)	124.6(5)	C(28)–C(29)–C(30)	120.4(7)

Table 2 Photophysical and electrochemical properties of complexes **1–5**

Complex	λ_{abs}[a] nm, $\varepsilon/10^4$ M^{-1} cm^{-1}	λ_{em}[b]/nm	HOMO/LUMO[c] [eV]	Band gap[c]/eV	E_{ox}[d]/V for $Ru^{2+/3+}$ (ΔE_p/mV)
1	245 (2.65), 287 (3.54), 295 (3.65), 368 (1.10), 401 (sh, 0.96), 490 (0.60), 552 (0.65)	702, 774	−7.32/−4.69	2.63	0.64 (68)
2	246 (3.16), 288 (4.64), 295 (5.12), 360 (1.32), 399 (1.18), 490 (0.88), 527 (0.87)	654, 710	−7.30/−4.67	2.63	0.70 (63)
3	244 (2.92), 286 (4.11), 294 (4.56), 344 (1.77), 408 (sh, 0.93), 495 (0.77), 519 (0.78)	707	−7.22/−4.70	2.52	0.74 (99)
4	241 (3.34), 282 (4.58), 292 (4.72), 356 (1.37), 395 (1.22), 484 (0.82), 524 (0.83)	653, 708	−7.35/−4.72	2.63	0.72 (69)
5	246 (0.75), 288 (4.96), 297 (5.47), 360 (2.70), 406 (sh, 1.55), 494 (1.01), 538 (0.93), 685 (sh, 0.085)	726	−6.63/−4.54	2.09	0.67 (25)

[a] Absorptions measured in ethanol. [b] Emissions measured in 2-methyltetrafuran glasses at 77 K. [c] DFT/B3LPY calculated values. [d] Recorded in MeCN with ferrocenium/ferrocene (Fc^+/Fc) as an internal reference and converted to NHE by addition of 490 mV.

chelating ligands were observed. For complexes **1–5**, the oxidation for anionic *C*,*N*-chelating ligands occurred at 0.99, 0.94, 0.89, 0.97 and 0.92 V, respectively. As expected, the peaks attributed to $Ru^{2+/3+}$ redox couples appeared at 0.64, 0.70, 0.74, 0.72 and 0.67 V, respectively, which are substantially more negative than that of $[Ru(bpy)_3]^{2+}$.[11,26] Moreover, $Ru^{2+/3+}$ redox couples with ΔE_p (25–99 mV) indicate that the processes are reversible (at least semi-reversible). It should be noticed that these cathodic shifts of $Ru^{2+/3+}$ redox processes are in agreement with an increase in the donor strength of cyclometalated ligands induced by anion binding and a decrease in the overall charge of these complexes.[16d,26] In these complexes, vinyl is an ideal electron delocalized channel. When it is used as a bridge between a pyridyl group and a substituted phenyl, the effect of electron donor strengths of the substituents is obvious. It can be seen in Table 2 that cyclometalated ligand in complex **5** renders the Ru(II) metal center easier to oxidize. The ligand involving a fluoride atom linked to phenyl shifts the oxidation potential to a bit more positive value. A similar trend for complex **1** and **2** was observed because methyl in complex **1** is a stronger electron donor than phenyl in complex **2**. These results are consistent with those cyclometalated ruthenium complexes involving 2-

Table 3 Calculated molecular orbital distributions and energy levels of complexes **1–5**

	HOMO−2	HOMO−1	HOMO	LUMO	LUMO+1	LUMO+2
1	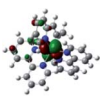 -7.90 (eV)	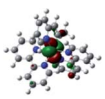 -7.70 (eV)	 -7.32 (eV)	 -4.69 (eV)	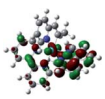 -4.56 (eV)	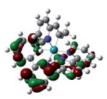 -3.86 (eV)
2	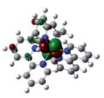 -7.90 (eV)	 -7.72 (eV)	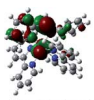 -7.30 (eV)	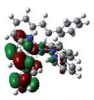 -4.67 (eV)	 -4.53 (eV)	 -3.84 (eV)
3	 -7.86 (eV)	 -7.77 (eV)	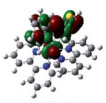 -7.22 (eV)	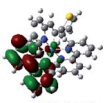 -4.70 (eV)	 -4.56 (eV)	 -3.88 (eV)
4	 -7.97 (eV)	 -7.78 (eV)	 -7.35 (eV)	 -4.72 (eV)	 -4.59 (eV)	 -3.90 (eV)
5	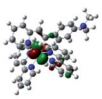 -7.55 (eV)	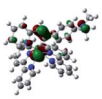 -7.26 (eV)	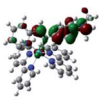 -6.63 (eV)	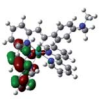 -4.54 (eV)	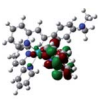 -4.39 (eV)	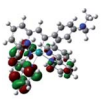 -3.72 (eV)

arylpyridines.[11,26b] In particular, a new reversible oxidation peak at 0.56 V (*versus* NHE) (0.07 V *versus* Ag^+/Ag) was observed for complex **5**, which can be assigned as *N*,*N*-dimethylphenyl group.[27] It indicated that there may be a possible intramolecular electron transfer from *N*,*N*-dimethylaminophenyl to Ru(III).[27]

Theoretical calculations

DFT calculations were carried out on complexes **1–5** to determine their electronic structures. Herein, calculated molecular orbital distributions and energy levels of complexes **1–5** are listed in Table 3. Obviously, the HOMOs of complexes **1–4** are primarily localized on ruthenium center and 2-vinylpyridine parts of the cyclometalated ligands. However, the HOMO of complex **5** is mainly delocalized on the double bond of vinyl and *N*,*N*-dimethylphenyl ring in the cyclometalated ligand with less distributions on Ru(II) and pyridine ring. It is clear that a set of π orbitals associated with 2-vinylpyridine parts of the cyclometalated ligands is located at slightly lower energy than vinylphenyl rings that comprise HOMO orbitals. In addition, all HOMO−1 and HOMO−2 orbitals primarily reside on Ru(II) center. And for complex **3**, the thienyl ring also makes a partial contribution to comprise the HOMO−2. As anticipated, all LUMOs of these complexes are associated with one or two neutral bipyridyl ligands. Herein, the corresponding energy gaps between the HOMO and LUMO are calculated to be 2.63, 2.63, 2.52, 2.63 and 2.09 eV, respectively. For vinylphenyl based cyclometalated complexes **2**, **4** and **5**, the decrease of the HOMO–LUMO gap resulted in an obvious red shift in the absorption spectrum of complex **5**.

TD-FDT calculations on optimized geometries in CH_2Cl_2 were then employed to model their corresponding absorption spectra. As suggested by TD-DFT calculations (see Table 4), the lowest singlet transitions responsible for the measured low-energy absorption bands of these complexes are assigned as S3 states, which are mainly composed of HOMO−1 → LUMO or HOMO−1 → LUMO+1 transitions. According to the orbital distributions, these absorption bands are mainly assigned as $[d\pi(Ru) \rightarrow \pi^*_{N\hat{N}}]$ MLCT transitions and $[\pi^*_{C\hat{N}} \rightarrow \pi^*_{N\hat{N}}]$ ligand-to-ligand charge-transfer (LLCT) transitions. For complexes **2**, **4** and **5**, TD-DFT shows that the absorption bands corresponding to S3 states are predicted at 523, 522 and 540 nm, respectively. It is consistent with the trend given by their experimental absorption spectra, in which their peaks occurred at 527, 524 and 538 nm, respectively.

pH sensitivity

Considering the deprotonation of C–H in *C*,*N*-chelating ligands for synthesizing cyclometalated ruthenium complexes,[10a,28,29a]

Table 4 Absorptions of complexes **1–5** in dichloromethane solutions from TDDFT calculations

Complex	States	λ (nm)	*E* (eV)	Oscillator	Main configurations	CI coeff.	Assignment
1	S1	614	2.02	0.0061	HOMO → LUMO	0.62	MLCT/LLCT
					HOMO → LUMO+1	0.25	MLCT/LLCT
	S2	605	2.0470	0.0002	HOMO → LUMO+1	0.62	MLCT/LLCT
	S3	535	2.3135	0.0310	HOMO−1 → LUMO	0.64	MLCT/LLCT
	S4	506	2.4496	0.0022	HOMO−2 → LUMO	0.50	MLCT/LLCT
	S5	503	2.46	0.084	HOMO−1 → LUMO+1	0.54	MLCT/LLCT
	S6	462	2.68	0.067	HOMO−2 → LUMO+1	0.46	MLCT/LLCT
2	S1	600	2.06	0.0002	HOMO → LUMO+1	0.54	MLCT/LLCT
	S2	596	2.0788	0.0045	HOMO → LUMO	0.55	MLCT/LLCT
					HOMO → LUMO+1	0.41	MLCT/LLCT
	S3	523	2.3687	0.0150	HOMO−1 → LUMO	0.65	MLCT/LLCT
	S4	490	2.53	0.056	HOMO−3 → LUMO+1	0.50	MLCT/LLCT
	S6	456	2.71	0.072	HOMO−2 → LUMO	0.51	MLCT/LLCT
3	S1	599	2.07	0.0004	HOMO → LUMO	0.44	MLCT/LLCT
					HOMO → LUMO+1	0.51	MLCT/LLCT
	S2	594	2.0854	0.0036	HOMO → LUMO	0.52	MLCT/LLCT
	S3	519	2.3888	0.0094	HOMO−1 → LUMO	0.66	MLCT/LLCT
	S4	489	2.54	0.054	HOMO−1 → LUMO+1	0.46	MLCT/LLCT
					HOMO−2 → LUMO+1	0.44	MLCT/LLCT
	S6	456	2.72	0.059	HOMO−2 → LUMO	0.45	MLCT/LLCT
					HOMO → LUMO+2	0.39	MLCT/LLCT
4	S1	598	2.07	0.0005	HOMO → LUMO	0.49	MLCT/LLCT
	S2	596	2.0790	0.0040	HOMO → LUMO	0.49	MLCT/LLCT
	S3	522	2.3729	0.0158	HOMO−1 → LUMO	0.65	MLCT/LLCT
	S4	490	2.5257	0.0285	HOMO−2 → LUMO+1	0.55	MLCT/LLCT
	S5	489	2.53	0.071	HOMO−1 → LUMO+1	0.49	MLCT/LLCT
	S6	456	2.72	0.072	HOMO−2 → LUMO	0.49	MLCT/LLCT
5	S1	637	1.94	0.0026	HOMO → LUMO	0.59	MLCT/LLCT
	S2	635	1.9511	0.0006	HOMO → LUMO+1	0.57	MLCT/LLCT
	S3	540	2.2943	0.0050	HOMO−1 → LUMO+1	0.45	MLCT/LLCT
	S4	535	2.31	0.011	HOMO−2 → LUMO	0.58	MLCT/LLCT
	S6	495	2.50	0.1002	HOMO−2 → LUMO+1	0.55	MLCT/LLCT

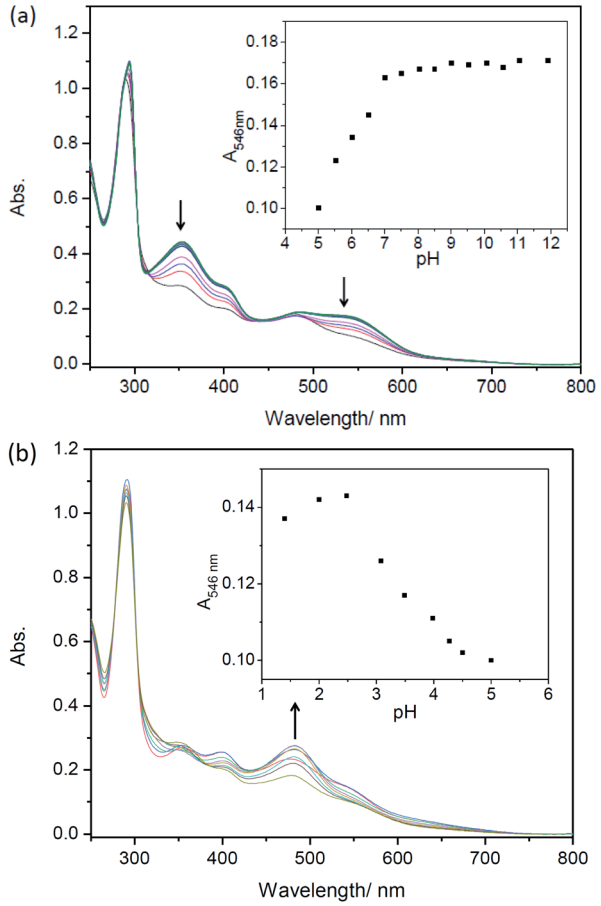

Fig. 3 Absorption spectral changes of complexes **5** (20 μM) after being incubated for 4 h in ethanol/Briton–Robinson buffer solutions (v/v = 1 : 2). (a) pH = 11.92–5.52; (b) pH = 5.00–1.40, respectively. Arrows show spectral changes upon decreasing pH. Inset: changes of absorption intensity at different pHs.

the presence of acids may lead to the intrusion of protons to carbanion, which could result in cleavages of Ru–C bonds and absorption spectral changes.[25,29] However, there are only a few reports on the protonation of cyclometalated ruthenium complexes.[25,29,30] Herein, UV-Vis absorption spectra of complexes **1–5** as a function of pH were then investigated. As shown in Fig. S19† and 3, in both alkaline and neutral environments, the intensities of absorption bands around 520 nm are almost unchanged for complexes **1–5**, which indicates the presence of Ru(II) → bpy CT originated from cyclometaled ruthenium complexes. Upon decreasing pH, the intensities of absorption bands around 520 nm are gradually decreasing and new peaks are centered at around 485 nm for these five complexes, indicating the cleavages of Ru–C bonds. Obviously, the protonation process involved an attack of H^+ to the anionic carbon atom, which weaken the Ru–C bond and resulted in great changes in MLCT absorptions. It is interesting that the newly formed band at 485 nm for complex **5** increased slightly in the intensities upon decreasing pH from 5.00 to 1.40 (Fig. 3b), which could be ascribed to the concurrent combination of one proton with *N*,*N*-dimethylamine.[31]

To better understanding the protonation process of these five cyclometalated complexes, absorption changes of $Ru(bpy)_2(ppy)^+$ (Hppy = 2-phenylpyrdine), $Ru(bpy)_2(dfppy)^+$ (Hdfppy = 2-(2,4-difluorophenyl)pyrdine) and $Ru(bpy)_2(thpy)^+$ (Hthpy = 2-(2-thienyl)pyridine) shared from our previous work[29b] are shown in Fig. S20.† It should be noted that the absorptions of complexes $Ru(bpy)_2(ppy)^+$, $Ru(bpy)_2(dfppy)^+$ and $Ru(bpy)_2(thpy)^+$ in acids are all centered at 450 nm and their corresponding products have been identified as $[Ru(bpy)_2(H_2O)_2]^+$ or $[Ru(bpy)_2X]^+$.[25,29] However, absorptions of complexes **1–5** in acids are around at 485 nm, which demonstrated that there may be different species in given acidic solutions rather than $[Ru(bpy)_2(H_2O)_2]^+$ or $[Ru(bpy)_2X]^+$. Then, MS spectra of these complexes were tracked after being incubated in methanol/HAc solution for 4 h. As shown in Fig. S21,† there is an evident peak occurring at *m*/*z* 563.18 in the MS spectrum of complex **1**, which could be attributed to the formation of $[MH^+–CH_3OH–H^+]^+$ (calc. *m*/*z* 563.63). For complexes **2–5** (Fig. S22–S25†), the peaks attributed to $[MH^+–CH_3OH–H^+]^+$ occurred at *m*/*z* 625.36 (calc. 625.71), 631.34 (calc. 631.64), 643.37 (calc. 643.69), 668.44 (calc. 668.77), respectively. These peaks demonstrated that the protonated species could have been formed as 2-alkenylpyridines attached to Ru(II) centers through N atoms when protons attacked carbonions and resulted in the cleavage of Ru–C bonds. Therefore, the different absorptions of complexes **1–5** in acidic solutions could be clearly explained by the presence of their protonated species. However, when these complexes were incubated in HAc/CH_3OH for a long enough time, complexes **1–4** were decomposed by losing *C*,*N*-chelating ligands and then

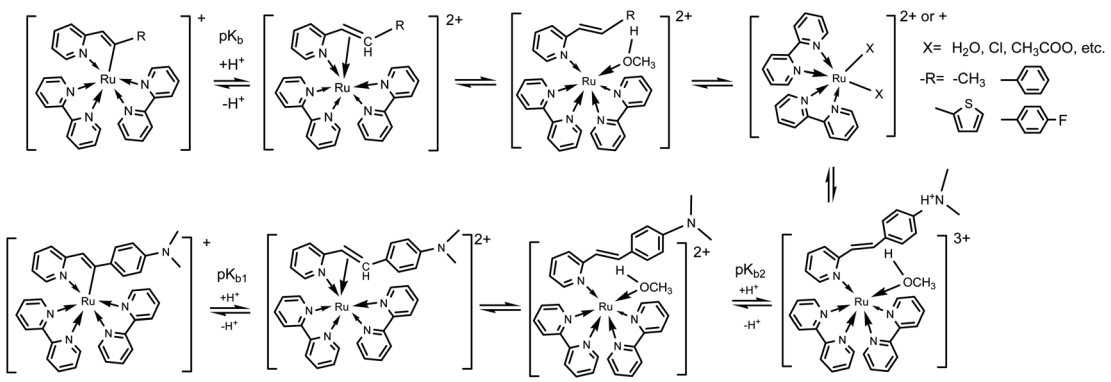

Scheme 2 The possible acid–base equilibria of complexes **1–5**.

Table 5 pK_b values of complexes **1–5** and three classical cyclometaleted ruthenium complexes

Complex	pK_b	Complex	pK_b
1	3.14 ± 0.02		
2	2.28 ± 0.03	$Ru(bpy)_2(ppy)^+$	4.02 ± 0.03
3	2.53 ± 0.02	$Ru(bpy)_2(thpy)^+$	4.99 ± 0.03
4	2.16 ± 0.02	$Ru(bpy)_2(dfppy)^+$	2.44 ± 0.02
5	2.86 ± 0.02		
	5.53 ± 0.06		

afforded $[Ru(bpy)_2CHCA–H^+]^+$ (Fig. S26–S29†). However, for complex **5**, the species $[MH^+–CH_3OH–H^+]^+$ was still observed (Fig. S30†). In addition, MS spectra of these complexes incubated in HCl/CH_3OH were also investigated, $[Ru(bpy)_2Cl]^+$ and $[Ru(bpy)_2CHCA–H^+]^+$ were found as the primary species for all complexes (Fig. S31–S35†). It should be noted that free 2-alkenylpyridines have been isolated and then characterized by ^{1}HNMR spectra for all these complexes in these acidic solutions including HAc/CH_3OH and HCl/CH_3OH. It can be seen that these five cyclometalated complexes are thermally unstable in strong acidic conditions. These complexes finally decomposed and gave off free *C*,*N*-ligands. Furthermore, the *C*,*N*-ligand of complex **5** was chosen to mix with $Ru(bpy)_2Cl_2$ in CH_3OH. As shown in Fig. S36,† some fragments that are the same as complex **5** in acid were observed after being treated by NaOH or Et_3N. According to these results of MS and UV-Vis spectra, the possible acid–base equilibria of these complexes could be depicted as Scheme 2.

Then, the ground-state protonation constant values (pK_b) of these five complexes were obtained by equation $pH = pK - lg[(A - A_0)/(A_f - A)]$ *via* their specific titration curves, respectively.[31] Herein, A_0 and A_f is the absorbance at the starting and ending pHs. As shown in Table 5, for complexes **1–4**, there is only one protonation process occurring at the carbanions in the alkenyls that are bonded to Ru(II) centers. However, for complex **5**, there are two protonation processes: the first is same to complexes **1–4**, the second is protonation of N atom on *N*,*N*-dimethylaminophenyl.[31] It can also be found that p*K* values depend on the electron properties of *C*,*N*-chelating ligands. For complexes involving vinylphenyl groups, a lower pK_b value was obtained for complex **4** which involved a fluorine atom as the electron-withdrawing substituent. However, with an electron-donating group, complex **5** afforded a higher pK_b value in its first protonation step. In comparison with phenyl attached to vinyl, methyl linked to vinyl is much stronger electron donator which resulted in a much higher pK_b value than others. The pK_b values of $Ru(bpy)_2(ppy)^+$, $Ru(bpy)_2(dfppy)^+$ and $Ru(bpy)_2(thpy)^+$ were also calculated and listed in Table 5, respectively. Obviously, an increase in the donor strength of the cyclometalated ligands could lead to easier decompositions of cyclometalated ruthenium complexes in acids.

Conclusion

In summary, five cyclometalated ruthenium complexes with 2-vinylpyridine derivatives as *C*,*N*-ligands were successfully synthesized and characterized. Their structures were identified by NMR, MS, FT-IR and elemental analysis spectra. Then, their photophysical properties were primarily studied by CV, UV-Vis and FL spectra combined with theoretical calculations. Furthermore, the influence of acids on these new cyclometalated ruthenium complexes was investigated by UV-Vis spectra. The regular changes in absorptions and different absorption bands from cyclometalated 2-arylpyridine ruthenium complexes could be attributed to the cleavage of Ru–C bonds without release of *C*,*N*-chelating ligands, which were further identified and confirmed by the MS spectra. Then, possible acid–base equilibria for these complexes were proposed.

Conflicts of interest

There are no conflicts to declare.

Acknowledgements

We are grateful for National Science Foundation of China (21971258), and thanks to the help of Analytical & Measuring Center, School of Pharmaceutical Sciences, South-Central University for Nationalities.

References

1 (*a*) J. Dupont, C. S. Consorti and J. Spencer, *Chem. Rev.*, 2005, **105**, 2527–2572; (*b*) M. Ghedini, I. Aiello, A. Crispini, A. Golemme, M. La Deda and D. Pucci, *Coord. Chem. Rev.*, 2006, **250**, 1373–1390.
2 A. C. Cope and R. W. Siekman, *J. Am. Chem. Soc.*, 1965, **87**, 3272–3273.
3 M. I. Bruce, *Angew. Chem., Int. Ed.*, 1977, **16**, 73–86.
4 R. Romeo, M. R. Plutino, L. M. Scolaro, S. Stoccoro and G. Minghetti, *Inorg. Chem.*, 2000, **39**, 4749–4755.
5 (*a*) J. B. Waern, C. Desmarets, L.-M. Chamoreau, H. Amouri, A. Barbieri, C. Sabatini, B. Ventura and F. Barigelletti, *Inorg. Chem.*, 2008, **47**, 3340–3348; (*b*) P. A. Scattergood, A. Sinopoli and P. I. P. Elliott, *Coord. Chem. Rev.*, 2017, **350**, 136–154; (*c*) J. Yu, M. Li, C. Xu, F. Meng, J. Cao, H. Tan and W. Zhu, *Dalton Trans.*, 2020, **49**, 8785–8790.
6 (*a*) G. Minghetti, A. Zucca, S. Stoccoro and M. A. Cinellu, *J. Organomet. Chem.*, 1994, **481**, 195–204; (*b*) M. R. Churchil, H. J. Wasserman and G. J. Young, *Inorg. Chem.*, 1980, **19**, 762–770; (*c*) K. Hiraki, Y. Fuchita and K. Takechi, *Inorg. Chem.*, 1981, **20**, 4316–4320.
7 (*a*) R. J. Foot and B. T. Heaton, *J. Chem. Soc., Dalton Trans.*, 1979, 295–298; (*b*) R. J. Foot and B. T. Heaton, *J. Chem. Soc., Chem. Commun.*, 1973, 838.
8 X. Yang, X. Xu, J. Zhao, J.-S. Dang, Z. Huang, X. Yan, G. Zhou and D. Wang, *Inorg. Chem.*, 2014, **53**, 12986–13000.
9 (*a*) B. M. Jennifer, S. Paulose, D. K. Rayabarapu, J.-P. Duan and C.-H. Cheng, *Adv. Mater.*, 2004, **16**, 2003–2007; (*b*) D. Wang, Y. Wu, H. Dong, Z. Qin, D. Zhao, Y. Yu, G. Zhou, B. Jiao, Z. Wu, M. Gao and G. Wang, *Org. Electron.*, 2013, **14**, 3297–3305; (*c*) D. M. Kang, J.-W. Kang, J. W. Park,

S. O. Jung, S.-H. Lee, H.-D. Park, Y.-H. Kim, S. C. Shin, J.-J. Kim and S.-K. Kwon, *Adv. Mater.*, 2008, **20**, 2003–2007; (*d*) S.-y. Takizawa, Y. Sasaki, M. Akhtaruzzaman, H. Echizen, J.-I. Nishida, T. Iwata, S. Tokito and Y. Yamashita, *J. Mater. Chem.*, 2007, **17**, 841–849.

10 (*a*) J.-P. Djukic, J.-B. Sortais, L. Barloy and M. Pfeffer, *Eur. J. Inorg. Chem.*, 2009, **7**, 817–853; (*b*) L. Labat, J.-F. Lamère, I. Sasaki, P. G. Lacroix, L. Vendier, I. Asselberghs, J. Pérez-Moreno and K. Clays, *Eur. J. Inorg. Chem.*, 2006, **15**, 3105–3113.

11 (*a*) F. Barigelletti, B. Ventura, J.-P. Collin, R. Kayhanian, P. Gavina and J.-P. Sauvage, *Eur. J. Inorg. Chem.*, 2000, **1**, 113–119; (*b*) M. L. Muro-Small, J. E. Yarnell, C. E. McCusker and F. N. Castellano, *Eur. J. Inorg. Chem.*, 2012, **25**, 4004–4011.

12 S. Ott, M. Borgström, L. Hammarström and O. Johansson, *Dalton Trans.*, 2006, **11**, 1434–1443.

13 (*a*) M. Borgström, S. Ott, R. Lomoth, J. Bergquist, L. Hammarström and O. Johansson, *Inorg. Chem.*, 2006, **45**, 4820–4829; (*b*) F. Barigelletti, L. Flamigni, M. Guardigli, A. Juris, M. Beley, S. Chodorowski-Kimmes, J.-P. Collin and J.-P. Sauvage, *Inorg. Chem.*, 1996, **35**, 136–142.

14 (*a*) I. S. Alpeeva, V. S. Soukharev, L. Aexandrova, N. V. Shilova, N. V. Bovin, E. Csöregi, A. D. Ryabov and I. Y. Sakharov, *JBIC, J. Biol. Inorg. Chem.*, 2003, **8**, 683–688; (*b*) A. D. Ryabov, V. S. Sukharev, L. Alexandrova, R. L. Lagadec and M. Pfeffer, *Inorg. Chem.*, 2001, **40**, 6529–6532.

15 (*a*) T. Bessho, E. Yoneda, J.-H. Yum, M. Guglielmi, I. Tavernelli, H. Imai, U. Rothlisberger, M. K. Nazeeruddin and M. Grätzel, *J. Am. Chem. Soc.*, 2009, **131**, 5930–5934; (*b*) P. G. Bomben, K. C. D. Robson, B. D. Koivisto and C. P. Berlinguette, *Coord. Chem. Rev.*, 2012, **256**, 1438–1450; (*c*) T.-D. Nguyen, Y.-P. Lan and C.-G. Wu, *Inorg. Chem.*, 2018, **57**, 1527–1534.

16 (*a*) X. Li, Y. Wu, Y. Liu, X. Zou, L. Yao, F. Li and W. Feng, *Nanoscale*, 2014, **6**, 1020–1028; (*b*) X. Li, K. Du, C. Xie, Y. Wu, B. Zhang and D. Tang, *Dalton Trans.*, 2020, **49**, 2024–2032; (*c*) X. Cheng, J. Li, X. Li, D. Zhang, H. Zhang, A. Zhang, H. Huang and J. Lian, *J. Mater. Chem.*, 2012, **22**, 24102–24108; (*d*) C. R. Wade and F. P. Gabbaï, *Inorg. Chem.*, 2010, **49**, 714–720; (*e*) H.-S. Lo, K.-W. Lo, C.-F. Yeung and C.-Y. Wong, *Anal. Chim. Acta*, 2017, **990**, 135–140.

17 Z. Lv, H. Wei, Q. Li, X. Su, S. Liu, K. Y. Zhang, W. Lv, Q. Zhao, X. Li and W. Huang, *Chem. Sci.*, 2018, **9**, 502–512.

18 (*a*) S. Aghazada, I. Zimmermann, V. Scutelnic and M. K. Nazeeruddin, *Organometallics*, 2017, **36**, 2397–2403; (*b*) H.-J. Park, K. H. Kim, S. Y. Choi, H.-M. Kim, W. I. Lee, Y. K. Kang and Y. K. Chung, *Inorg. Chem.*, 2010, **49**, 7340–7352; (*c*) X. Xie and H. V. Huynh, *Org. Chem. Front.*, 2015, **2**, 1598–1603; (*d*) J. Soellner, I. Císařová and T. Strassner, *Organometallics*, 2018, **37**, 4619–4629.

19 V. S. Soukharev, A. D. Ryabov and E. Csöregi, *J. Organomet. Chem.*, 2003, **668**, 75–81.

20 S. Fernandez, M. Pfeffer, V. Ritleng and C. Sirlin, *Organometallics*, 1999, **18**, 2390–2394.

21 X. Zhou, X. Li, Y. Liu, R. Li, K. Jiang and J. Xia, *Org. Electron.*, 2015, **25**, 245–253.

22 (*a*) L. J. Bourhis, O. V. Dolomanov, R. J. Gildea, J. A. K. Howard and H. Puschmann, *Acta Crystallogr., Sect. A: Found. Adv.*, 2015, **71**, 59–71; (*b*) O. V. Dolomanov, L. J. Bourhis, R. J. Gildea, J. A. K. Howard and H. Puschmann, *J. Appl. Crystallogr.*, 2009, **42**, 339–341; (*c*) G. M. Sheldrick, *Acta Crystallogr., Sect. C: Struct. Chem.*, 2015, **71**, 3–8.

23 X. Su, R. Hu, X. Li, J. Zhu, F. Luo, X. Niu, M. Li and Q. Zhao, *Inorg. Chem.*, 2016, **55**, 745–754.

24 X. Su, X. Li, T. Ding, G. Zheng and Z. Liu, *J. Organomet. Chem.*, 2015, **781**, 59–64.

25 P. Reveco, R. H. Schmehl, W. R. Cherry, F. R. Fronczk and J. Selbin, *Inorg. Chem.*, 1985, **24**, 4078–4082.

26 (*a*) P. Reveco, W. R. Cherry, J. Medley, A. Garber, R. J. Gale and J. Selbin, *Inorg. Chem.*, 1986, **25**, 1842–1845; (*b*) P. G. Bomben, B. D. Koivisto and C. P. Berlinguette, *Inorg. Chem.*, 2010, **49**, 4960–4971.

27 (*a*) R. Argazzi and C. A. Bignozzi, *J. Am. Chem. Soc.*, 1995, **117**, 11815–11816; (*b*) X. Li, J. Gui, H. Yang, W. Wu, F. Li, H. Tian and C. Huang, *Inorg. Chim. Acta*, 2008, **361**, 2835–2840; (*c*) N. Hirata, J.-J. Lagref, E. J. Palomares, J. R. Durrant, M. K. Nazeeruddin, M. Gräztel and D. D. Censo, *Chem.–Eur. J.*, 2004, **10**, 595–602.

28 B. Li, T. Roisnel, C. Darcel and P. H. Dixneuf, *Dalton Trans.*, 2012, **41**, 10934–10937.

29 (*a*) E. C. Constable, *Polyhedron*, 1984, **3**, 1037–1057; (*b*) X. Su, R. Zeng, X. Li, W. Dang, K. Yao and D. Tang, *Dalton Trans.*, 2016, **45**, 7450–7459.

30 (*a*) E. C. Constable, S. J. Dunne, D. G. F. Rees and C. X. Schmitt, *Chem. Commun.*, 1996, **10**, 1169–1170; (*b*) C. Moorlag, O. Clot, M. O. Wolf and B. O. Patrick, *Chem. Commun.*, 2002, 3028–3029; (*c*) C. Moorlag, M. O. Wolf, C. Bohne and B. O. Patrick, *J. Am. Chem. Soc.*, 2005, **127**, 6382–6393.

31 (*a*) F. Liu, K. Wang, G. Bai, Y. Zhang and L. Gao, *Inorg. Chem.*, 2004, **43**, 1799–1806; (*b*) T. T. Meng, H. Wang, Z. B. Zheng and K. Z. Wang, *Inorg. Chem.*, 2017, **56**, 4775–4779; (*c*) X. L. Zhao, Z. S. Li, Z. B. Zheng, A. G. Zhang and K. Z. Wang, *Dalton Trans.*, 2013, **42**, 5764–5777.